Characterization of Acridine Species Adsorbed on $(NH_4)_2SO_4$, SiO_2, Al_2O_3, and MgO by Steady-State and Time-Resolved Fluorescence and Diffuse Reflectance Techniques

Ideliz Negrón-Encarnación, Rafael Arce,* and Maricruz Jiménez

University of Puerto Rico, Río Piedras Campus, P.O. Box 23346, San Juan, Puerto Rico 00931

Received: September 17, 2004; In Final Form: October 26, 2004

The ground- and excited-state species of acridine adsorbed on $(NH_4)_2SO_4$, SiO_2, Al_2O_3, and MgO surfaces were investigated in order to determine the precursor species and electronic states responsible for acridine photodegradation on particles serving as models of atmospheric particulate matter. The species present on each solid surface were characterized by comparing the steady-state absorption and fluorescence spectra, time-resolved fluorescence, and absorption measurements on acridine in solution with those corresponding to adsorbed acridine. On silica, the ground-state species present were hydrogen-bonded, neutral, and protonated, while on alumina hydrogen-bonded and neutral species were identified. A comparison of the protonated acridine absorption and emission intensities on silica and alumina with those observed for acridine in acidic water demonstrated that the emission on the surfaces is higher than expected. This was interpreted as resulting from photoprotolytic reactions on silica and alumina. For acridine adsorbed on ammonium sulfate, protonated acridine was the only adsorbed species identified. Since, at a similar ground-state absorbance, the fluorescence intensity of acridine on ammonium sulfate was smaller than for acridine in acidic water, the quenching of the excited state or a rapid photochemical reaction with the surface was proposed. On magnesium oxide, the presence of neutral and hydrogen-bonded acridine species were characterized from the two-component analysis of the fluorescence, the triplet−triplet absorption decay curves, and the time-resolved emission spectra at different time delays. As demonstrated in these studies, acridine adsorbed species and their decay pathways depend on the acidic properties of these models of atmospheric particulate matter. In addition, a comparison of the photodegradation rates of acridine on the different solids tested is presented and discussed in terms of the nature of the species and their decay pathways.

I. Introduction

The composition of the atmospheric particulate matter is of great concern to human health because its deposition in the respiratory tract has been related to several diseases.[1,2] These particles have been associated with the presence of adsorbed or absorbed polycyclic aromatic compounds (PACs), in particular with their oxidation products.[3−5] Studies have demonstrated that the oxidation products of PACs can be more harmful than the parent compound.[2,3,5] As a consequence, there is great interest in elucidating the transformation routes of adsorbed PACs. Acridine (Figure 1), an aza-heterocyclic aromatic compound, is found in the troposphere as a result of the incomplete combustion of propane gas, diesel, and coal exhaust.[6,7] Due to the low value of its Henry's constant ($H = 4 \times 10^{-7}$ atm·m^3/mol), it is readily adsorbed on atmospheric particulate matter.[8] Although acridine is also found in water, on the basis of the magnitude of its organic carbon normalized sorption coefficient (K_{oc}), it is readily immobilized in the soil and sediment.[9,10] Because the toxicity of acridine solutions increases after irradiation with 350 nm light, it is of interest to study if similar transformations can occur in the adsorbed state.[5]

Luminescence and triplet−triplet absorption studies of acridine in different solutions have demonstrated that the decay pathways of its excited states depend on the nature of acridine species present (neutral, hydrogen-bonded, or protonated), and the environment (protic, aprotic, or in hydrogen donor solvents). Neutral acridine (in basic water, $\phi_F = 0.33$)[11] and hydrogen-bonded acridine (in methanol, $\phi_F = 0.02$)[12] species present lower fluorescence quantum yields (ϕ_F) than protonated acridines (in acidic water, $\phi_F = 0.66$).[11] Intersystem crossing quantum yields of 0.39 [12] and 0.42 [13] have been reported for neutral acridine in alkaline water and for hydrogen-bonded acridine in ethanol respectively, while protonated acridine presented a smaller intersystem crossing quantum yield. These results indicate that the decay pathways from the acridine excited states depend on the type of acridine species present. Therefore, to be able to interpret the photochemical transformations and rates of photodegradation of acridine adsorbed on models of atmospheric particulate matter, it is necessary to determine the nature of the species of acridine (neutral, hydrogen-bonded, or protonated) present on these.

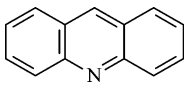

Figure 1. Schematic representation of acridine.

The major chemical components of atmospheric particulate matter are sulfate, nitrate, and ammonium salts and organic and elemental carbon.[14] Other inorganic oxides such as SiO_2, Al_2O_3, MgO, CaO, and Fe_2O_3 are also found.[14] In this study $(NH_4)_2SO_4$, SiO_2, Al_2O_3, and MgO were used as models of atmospheric particulate matter. The silica surface consists of an interconnected network of siloxane (Si−O−Si) linkages, a variety of silanol groups (Si−OH) and physically adsorbed water.[15] The

* To whom correspondence should be addressed. E-mail: rarce@goliath.cnnet.clu.edu.

10.1021/jp045758+ CCC: $30.25
Published on Web 01/12/2005

most effective binding agent to lone pairs of the heteroatom in aza-arenes are the silanol groups. There are generally 4−5 silanols/nm^2.[15] On the surface of alumina, hydroxyl groups attached to aluminum and physically adsorbed water molecules are found. There are 12−13 hydroxyls/nm^2, and their properties are determined by their coordination to aluminum atoms and net charge.[15] The magnesium oxide surface consists of two types of hydroxyl groups formed from the dissociation of water into OH groups and protons, which are then adsorbed on the magnesium and oxygen ions to produce $Mg_{surface}$−OH and $O_{surface}$−H groups.[16] In addition, physisorb water molecules are present.[17] Ammonium sulfate is a hygroscopic salt. The hydrogens of the ammonium ions form hydrogen bonds with water, resulting in a hydrated surface.[17] Due to differences in the quantity and acidity of the hydroxyl groups on each solid surface, different acridine species can exist on each of these atmospheric particulate matter models. In the present study the adsorbents were not activated by heat treatment because we attempted to match as closely as possible the ambient conditions in which these substrates are found.

Different acridine species (neutral, AN; hydrogen-bonded, AN···HO; and protonated, ANH^+) display characteristic absorption spectra,[18,19] emission spectra,[18,19] fluorescence lifetimes,[18−20] and triplet−triplet adsorption spectra.[21,22] Therefore, the different acridine-adsorbed species can be characterized using steady-state absorption and fluorescence, fluorescence lifetimes, and time-resolved diffuse reflectance laser flash measurements. In this paper, we present and compare some photophysical properties, measured by these techniques for acridine in water at different pHs, methanol, and hexane, and for acridine adsorbed on models of atmospheric particulate matter.

Besides being an organic pollutant, acridine has been used as a fluorescent probe to examine surface sites on inorganic oxides on the basis of its strength of adsorption and acid−base interactions between its nitrogen heteroatom and surface sites. The study of surface sites on inorganic oxides is relevant because of their use as adsorbents, active catalysts, catalyst supports, and insulators. Acridine has been used as a probe to study the surface sites on alumina and silica (activated at different heat pretreatment temperatures) by absorption,[23−26] fluorescence,[23−26] and time-resolved diffuse reflectance spectroscopy[26] techniques. Steady-state diffuse reflectance and fluorescence studies have demonstrated that protonated and neutral acridine species are formed on unactivated γ-alumina (Merck).[26,27] In the alumina made by another chemical company (Degussa), the main species present were neutral acridines; in addition, photoprotolytic reactions occurred, resulting in the formation of protonated acridine species from acridines in their singlet excited state.[27] After thermal pretreatment of these aluminas at 100 °C, the main adsorbed species were protonated acridines. The authors suggested that the acidity of the alumina was higher when physiadsorbed water was removed, resulting in higher yields of formation of protonated acridines than on the unactivated surfaces.[27] The adsorption and emission spectra of acridine on silica gel pretreated at different temperatures (T_a) provided evidence of the presence of protonated acridines at low T_a (100 or 180 °C), and a larger yeld of neutral acridine species at higher T_a (300−800 °C).[23,25−28] In addition, the formation of singlet excited protonated acridine has been reported on silica.[23,25,27,29] These studies have demonstrated that the type of the acridine species produced on the inorganic solids depends on the acidic properties of the substrate and its water content.

The time-resolved diffuse reflectance (TRDR) spectra of acridine on thermally pretreated silica and alumina surfaces have been reported.[26] For acridine on silica pretreated at low temperatures, delay fluorescence has been observed as a result of a triplet−triplet annihilation process. The TRDR spectra was only seen at high pretreatment temperatures at which dehydroxylation occurred because of the increase of the activation barrier for the mobility of the acridine species with an increase in dehydroxylation.[26] On alumina, acridinium ions have been identified as the main species present at low pretreatment temperatures.[26] Studies on thermally activated silica and alumina have been focused mainly on the determination of the surface sites responsible for their catalytic activity, using acridine as a probe. These surfaces can be activated by heat treatment, dehydroxylation, and loss of water molecules adsorbed on the surface. Activation at low temperatures (usually 100 °C) may not produce dehydroxylation but rather result in water loss. On unactivated surfaces, water is expected to be present, a condition that more closely mimics atmospheric conditions. In addition, such studies have not been done using other models of fine atmospheric particulate matter such as magnesium oxide and ammonium sulfate surfaces. These inorganic solids represent a higher fraction in the composition of the fine atmospheric particulate matter than silica and alumina.[14]

II. Experimental Section

A. Reagents and Sample Preparation. Acridine (99.2% of purity by HPLC), chromatographic grade 60 Å silica and magnesium oxide were obtained from Aldrich, alumina from Sigma Chemical, ammonium sulfate from Alfa AESAR, and the solvents (optima grade) from Fisher. The water content (Galbraith Laboratories) and BET surface area (Quantachrome Instruments) analysis were done for all the solids tested. The results are as follows: ammonium sulfate (0.10% water, 2.196×10^{-2} m^2/g); alumina (8.59% water, 1.960×10^2 m^2/g); silica (9.53% water, 4.100×10^2 m^2/g); magnesium oxide (9.67% water, 1.016×10^2 m^2/g). The adsorbed samples were prepared by adding a measured amount of a solution of acridine in hexane of a known concentration to a weighted amount of the adsorbent to obtain the desirable loading concentration. After the complete adsorption of the acridines the solvent was removed by rotoevaporation. The time at which complete adsorption of acridine occurred was determined from absorption measurements of the solution of acridine in hexane at different times after its addition to the adsorbent particles. For sensitization studies, an acridine solution in hexane was equilibrated with the solid until complete adsorption, an aliquot of a benzophenone solution in hexane was added, and the hexane was rotoevaporated. The reproducibility of sample preparation and of the loading procedure was established from initial fluorescence or diffuse reflectance intensities. The surface loadings used were lower than a monolayer as determined from Langmiur adsorption isotherms. To determine the acridine adsorption isotherms, the change in concentration of acridine in hexane was used as a quantity proportional to the amount of adsorbed species. The Langmiur adsorption isotherm of acridine on ammonium sulfate from a hexane solution (Figure 2) shows that at concentrations of adsorbed acridine above 6×10^{-6} mol/g, the surface sites were saturated and a monolayer was formed. For acridine on MgO, Al_2O_3, and SiO_2 the formation of a monolayer was not observed at the highest change in concentration (5×10^{-5} mol/g) observed.

B. Diffuse Reflectance and Emission Spectroscopy. Fluorescence spectra were recorded with a SLM AMINCO spectrofluorometer model MCN320 upgraded with photon-counting electronics of ISS using an excitation and emission slits width

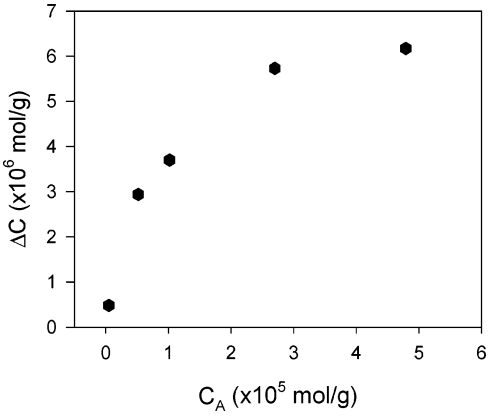

Figure 2. Adsorption isotherm of acridine in hexane on ammonium sulfate at 23 °C.

of 4 nm. Diffuse reflectance spectra were obtained with a Varian Cary 1E double beam spectrophotometer with an integrating sphere. Diffuse reflectance spectra of acridine adsorbed on the solids surface obtained under a nitrogen atmosphere presented a lower absorbance intensity than those taken under an oxygen atmosphere due to the quenching of the fluorescence emission by oxygen. Because of the absence of a monochromator placed before the detector in the integrating sphere, the fluorescence photons could reach the detector. The fluorescence intensity of acridine increased under a nitrogen atmosphere due to the lower frequency of quenching by oxygen; therefore, a larger number of photons reached the diffuse reflectance detector than under an oxygen atmosphere when the fluorescence is quenched to a higher extent. As a consequence, the apparent absorbance intensity under a nitrogen atmosphere was higher than that under an oxygen atmosphere. However, the relative intensities of the bands did not change substantially in the presence of oxygen, demonstrating that it does not affect the absorbance properties of acridine (see Supporting Information). The percent that the absorbance intensity decreased under a nitrogen atmosphere with respect to an oxygen atmosphere was 55% on silica, 20% on alumina, and 5% on magnesium oxide. For acridine on ammonium sulfate the intensity of the diffuse reflectance spectra was independent of the gaseous atmosphere, possibly because of its low-emission intensity on that surface.

C. Time Domain Fluorescence Spectroscopy. The fluorescence decay curves and the time-resolved emission spectra of acridine were obtained with a N_2 laser model GL-3300 from Photon Technology International (PTI) using an excitation wavelength of 337 nm (pulse width of 2 ns) and a pulse frequency of 10 Hz. The emission wavelength was dispersed by the monochromator of the SE-900 PTI spectrofluorometer and detected by a photomultiplier tube model R1527P of PTI. Time-correlated single-photon-counting technology was employed. The data were analyzed using Time Master software version 1.2 from PTI. The kinetic decay curves were analyzed by deconvolution with the instrument response function.

D. Laser Flash Spectroscopy. Transient intermediates were generated with the third (355 nm) or fourth (266 nm) harmonic output of a Continuum Surelite II laser. Transient species in solution were monitored at right angles to the unfocused laser beam using a 150 W xenon arc lamp (Oriel Corp.) as the analyzing light. Transient species adsorbed on the surface were monitored using the diffuse reflected radiation from a 300 W xenon arc lamp (Oriel Corp.) positioned at 90° relative to the cell surface, while the unfocused laser beam was at 30° from the cell surface. The wavelengths from the probe beam were dispersed with a monochromator and detected with an electron photomultiplier detector. Output from the photomultiplier was digitized with a 500 MHz bandwidth oscilloscope, model 9360 (LeCroy Corp.). The spectrokinetic system was controlled with Labview 5.1-based application software (National Instrument, Austin TX). The T−T absorption spectra of acridine was not observed in the presence of oxygen; therefore, the acridine samples in solution and on the solids where purged with nitrogen to avoid triplet quenching by oxygen. Other authors had to use freeze−pump−thaw cycles or high vacuum to degas the samples.[11,12,22] Differences in the lifetimes of triplet-state acridine obtained in these studies with those previously reported could be due to the lower efficiency of removing oxygen by a N_2 gas flow than by a high-vacuum degassing procedure. Triplet−triplet energy-transfer experiments from benzophenone to acridine were performed to determine the presence of ANH^+. Benzophenone was selected as the sensitizer due to its high intersystem crossing quantum yield, the presence of a triplet state of higher energy than acridine, the absence of T−T absorbance in the acridine absorption region, and its significant absorbance at the 266 nm laser excitation wavelength. In the sensitization process the triplet state of benzophenone was produced after excitation with a 266 nm high-intensity pulse.

E. Photolysis Studies. The samples were irradiated with an Oriel 300 W Xe(Hg) lamp. A water filter was used to eliminate IR radiation, and a broad band Corning 7-51 filter was used to irradiate exclusively the acridine band at 355 nm. The lamp intensity reaching the sample was 1.1×10^{-2} W/cm^2. The photodegradation of acridine adsorbed on the solid surfaces was followed by diffuse reflectance techniques (for AN on MgO) or front face fluorescence (for AN on $(NH_4)_2SO_4$, SiO_2, and Al_2O_3) intensity measurements before and after the irradiation of the sample inside a stationary quartz cell. In solution, the photodegradation rate of acridine was followed by the analysis of the chromatographic peak area of acridine. These studies were done under air, N_2, or O_2 atmospheres.

III. Results and Discussion

A. Ground-State Absorption Spectra. The UV−vis absorption spectra of acridine are the result of three or four transitions, depending on the nature of the solvent. These spectra include one in the UV-C and two (for protonated species) or three (for neutral species) in the UV-A−vis wavelength regions.[18,19] The two highest energy transitions at 250 and 355 nm are $\pi \rightarrow \pi^*$ in nature while the lowest energy transitions (375 or 430 nm) could be $n \rightarrow \pi^*$ or $\pi \rightarrow \pi^*$, depending on the polar nature of the solvent and the acridine species present.[18,19] In protic polar solvents, the transition to the first excited singlet state decreases ~10 nm with respect to that in aprotic nonpolar solvents. In acidic water, the $n \rightarrow \pi^*$ transition disappears due to the protonation of the acridine nitrogen. The first and second (π, π^*) excited singlet states of acridine have been denominated as L_a and L_b, respectively, according to the perimeter free electron orbital model.[30] As the water pH drops, the L_a transition shifts to a higher wavelength (from 380 to 430 nm) due to the protonation of acridine ($pK_a = 5.45$).[31] Thus, the wavelength position of this band is a good indicator of the presence of protonated acridine, ANH^+. For hydrogen-bonded (in methanol) and neutral (in hexane) acridine species, the $S_0 \rightarrow S_1$ transitions are not well-resolved, as these appear at 380 and 375 nm, respectively. Therefore, the exclusive presence of either of these two species could not be clearly established.

The absorption spectrum of acridine adsorbed on ammonium sulfate is shown in Figure 3a. This is very similar to that of acridine in water at pH 2.5. The L_a band was observed at the

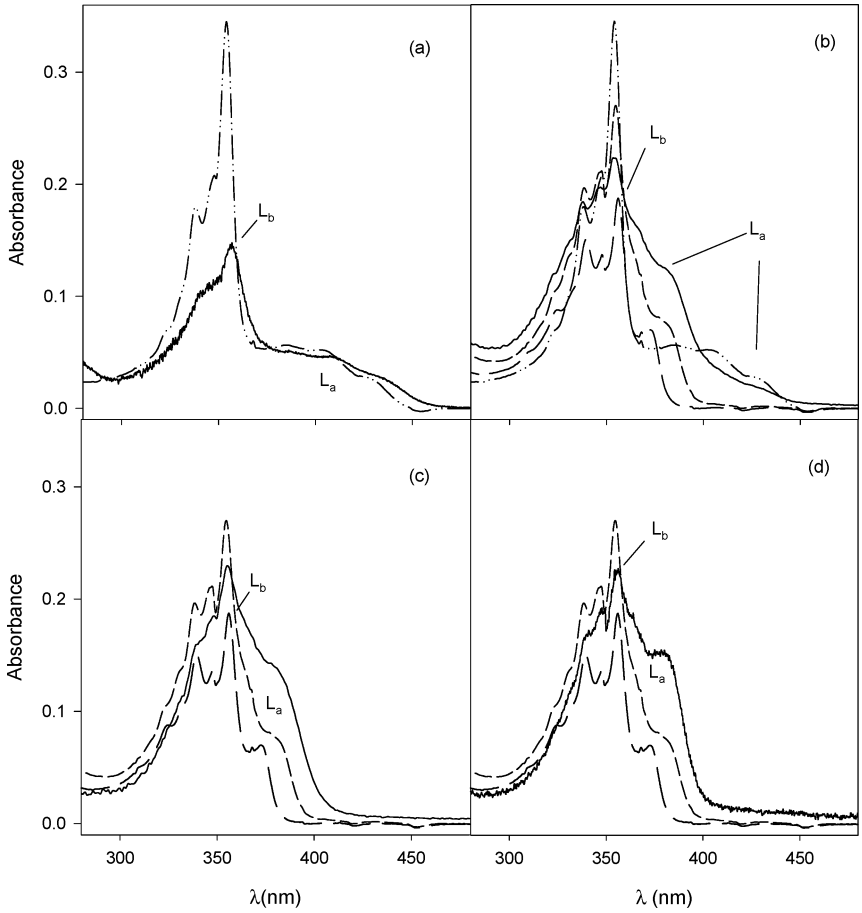

Figure 3. Diffuse reflectance spectra of acridine adsorbed on the following solids (—): (a) 5×10^{-8} mol/g on $(NH_4)_2SO_4$; (b) 2×10^{-7} mol/g on SiO_2; (c) 6×10^{-7} mol/g on Al_2O_3; (d) 5×10^{-6} mol/g on MgO. Absorption spectra of 2.5×10^{-5} M of acridine in the following solutions are presented for comparison: water at pH of 2.5 (— •• —), methanol (--), and hexane (— —).

430 nm region, although a shoulder on this band in the 380 nm region was not observed. A L_a band in the 400−450 nm region is strong evidence of the presence of a ground-state acridine-protonated species. For acridine adsorbed on silica (Figure 3b), two L_a bands in the 385 and 430 nm regions were observed. Contributions to the spectra from the absorption of protonated species can be clearly established from the absorption band at 430 nm, while the presence of the hydrogen-bonded and/or neutral acridines can be inferred from the band at ∼385 nm. On alumina and magnesium oxide (Figure 3c,d), acridine presented a L_a band in the 380 nm region, suggesting the presence of the neutral and/or hydrogen-bonded acridine species on these surfaces. Contributions from the protonated species were not observed due to the absence of a L_a band in the 400−450 nm region as is normally seen for acridine at pH 2.5 (Figure 3a). Previous studies have shown that protonated species are present on 100 °C pretreated alumina. However, on untreated alumina the ANH^+ species were at lower concentration or absent.[26,27] In our studies, the alumina was not thermally activated and protonated acridines were not observed. A dependence of the formation of ANH^+ with the water content was suggested by Rempfer and co-workers.[27] The alumina used in our studies was exposed to atmospheric water and not thermally treated. Older and newer alumina samples from the same chemical company (Sigma Chemical) were used because these had different water contents due to their different exposure times to atmospheric water. The diffuse reflectance spectra of acridine on these aluminas containing two different water percents were recorded to establish the effect of water content in the yield of the acridine species. For the older alumina (8.59% of water) the neutral species were present (Figure 3c), while for the newer alumina (2.27% of water) the neutral and protonated species were observed. Therefore, the interaction of acridine with the acidic sites on alumina decreased as the water content increased. However, the formation of ANH^+ may also depend on the acidity of the surface. This was estimated by measuring the pH of water in contact with the alumina powder. For silica the surface pH was determined as 6.6, allowing for the possible formation of protonated species on this surface. The alumina was pH 7.7, more basic than the pH of silica. Therefore, the protonation of acridine under dark conditions was more favorable for acridine adsorbed on silica than on the alumina surface, as demonstrated by the fact that the absorption band associated with protonated acridine was not seen on alumina.

The diffuse reflectance spectra of acridine on the different solids show a similar absorbance, but they were obtained from samples with different surface loadings. The acridine surface loading was in the following order: ammonium sulfate < silica < alumina < magnesium oxide. The degree of attenuation of the diffuse reflected light depends on the absorption coefficient of the sample and penetration depth. The similar absorbances at different surface loading are related to the presence of protonated acridines since these have a higher absorption coefficient than the neutral species. At 355 nm the absorption coefficient of the ANH^+ species is 2.5 times higher than that for the neutral species. Because acridine on ammonium sulfate is protonated while on alumina is not, it presented a higher absorbance on ammonium sulfate than on alumina. Therefore, different absorbance on the surfaces tested will be observed at

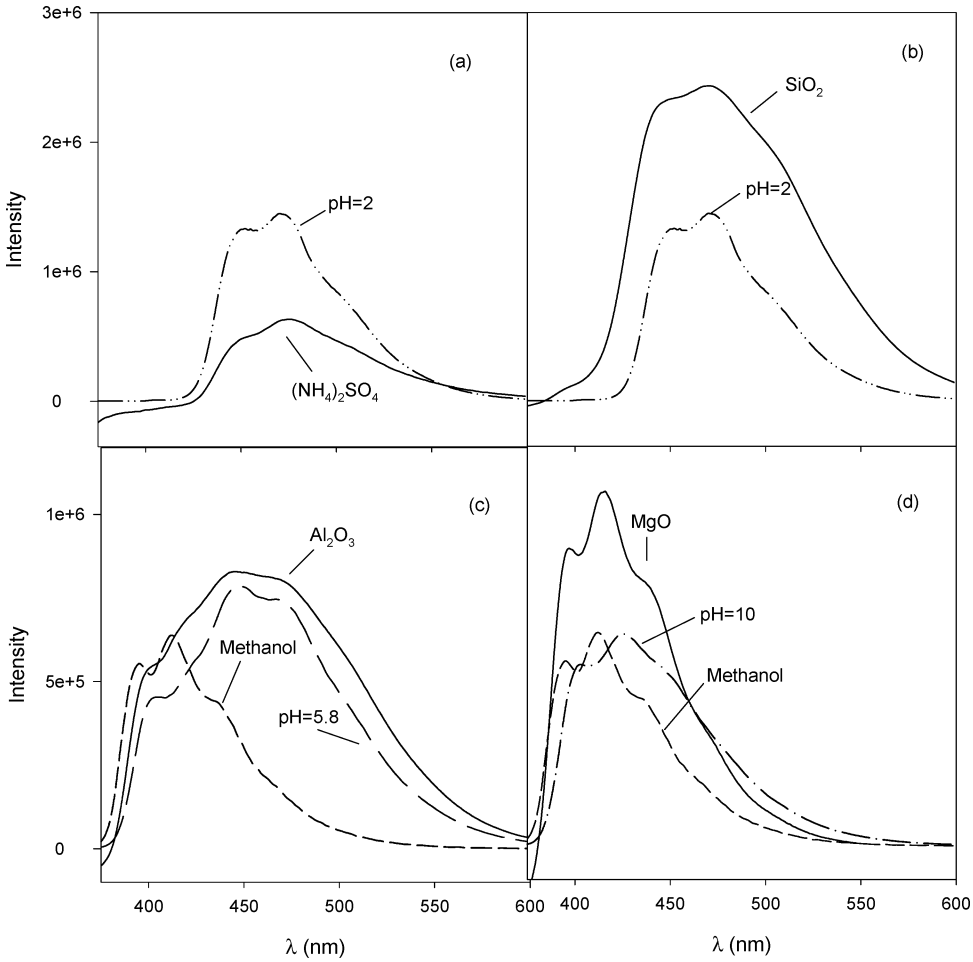

Figure 4. Emission spectra of acridine adsorbed on the following solids (—): (a) 5×10^{-8} mol/g on $(NH_4)_2SO_4$; (b) 2×10^{-7} mol/g on SiO_2; (c) 6×10^{-7} mol/g on Al_2O_3; (d) 5×10^{-6} mol/g on MgO. Emission spectra of 2.5×10^{-5} M of acridine in the following solutions are presented for comparison: water at pH of 2.5 (— ·· —); water at pH of 5.8 (— —); water at pH of 10 (— · —) and methanol, intensity × 10 (--). The excitation wavelength was 355 nm.

similar surface loadings. However, similar absorbances were observed at differences of 2 orders of magnitude in the surface loading, which suggest that these differences are not only due to the absorption coefficient on the adsorbed species. These differences could also be related to the penetration depth of the incident light, which depends on scattering and transmission properties of the solids.

B. Steady-State Emission Spectra. The steady-state emission spectra of adsorbed acridine were used to establish the nature of the excited-state species present on each model surface. According to the diffuse reflectance spectra, adsorbed ground-state acridine could exist as AN, AN···HO, and/or ANH^+. These may be the same species observed in the fluorescence spectra, unless photochemical reactions of the acridine excited state change their nature. The shift of the acridine emission band from 425 to 470 nm as the pH of its environment decreased from 6.6 to 4.8 has been used as an indication of the protonation of acridine.[29] In our work, at pH 10 neutral acridine (AN) presented an emission band with a maximum at 425 nm, while, in methanol, the hydrogen-bonded species AN···HO exhibited the emission maximum at 414 nm.

Acridine adsorbed on $(NH_4)_2SO_4$ (Figure 4a, $\lambda_{max} = 475$ nm) and on silica gel (Figure 4b, $\lambda_{max} = 469$ nm) presented emission bands in the same wavelength region as that observed for acridine in water at pH 2.5 ($\lambda_{max} = 472$ nm). Therefore, we propose that on these surfaces the major species of acridine in the singlet excited state was the protonated form. In the case of acridine adsorbed on ammonium sulfate, the characterized ground- and excited-state species present were in their protonated form. On silica gel as the adsorbent, while the absorption spectrum presented contributions from protonated, hydrogen-bonded, and/or neutral acridine species, acridine's emission spectrum was characteristic of the protonated form, ANH^+. These results suggested that on silica gel, acridine could undergo an excited-state proton-transfer reaction. The excitation spectrum of acridine on silica (Figure 5) was similar to the diffuse reflectance spectra, suggesting that the emitting species were the protonated, hydrogen-bonded, and/or neutral acridine. This suggests that the low contribution of neutral species to the emission spectra could be the result of a photoprotolytic reaction. Indeed, the excitation spectra are not strong evidence that a photoprotolytic reaction occurred, but its possibility should not be excluded. This photoprotolytic reaction with hydroxyl silica groups has been reported in heat-pretreated silica surfaces at 180 °C.[23−25]

When adsorbed on Al_2O_3, acridine presented an emission spectrum (Figure 4c, $\lambda_{max} = 444$ nm) very similar to that observed in an aqueous solution at pH 5.8. At this pH the ratio of $[ANH^+]/[AN]$ is 0.44. Thus, on the basis of the fluorescence spectrum of acridine at a pH of 5.8, we proposed that AN and ANH^+ species were present on the alumina surface. The presence of hydrogen-bonded species on alumina cannot be totally discarded because in methanol ($\lambda_{max} = 414$ nm) these emit on the blue side of the emission spectra of acridine on

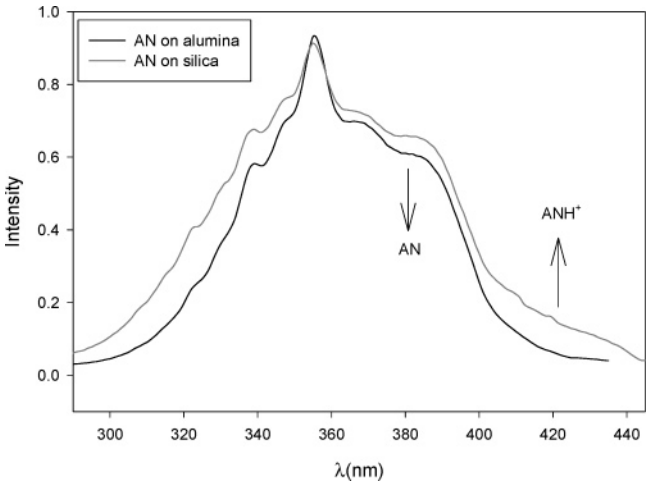

Figure 5. Excitation spectra of 5×10^{-7} mol/g acridine on alumina (Em 450 nm) and silica (Em 470 nm).

alumina. Since only contributions from neutral and/or hydrogen-bonded species were observed in the absorption spectra on alumina, the contribution from the protonated species to the emission spectrum suggested that an efficient photoprotolytic reaction was occurring on this surface (eq 1). Moreover, the excitation spectra of acridine on alumina did not show the contribution of ANH^+ species to the emission, while the emission spectra did (Figure 5). This demonstrated the participation of singlet excited-state proton addition reaction in the formation of protonated acridine. Indeed, the formation of singlet excited ANH^+ has been reported in not-pretreated alumina.[27]

$$AN\cdots HO-Al + h\nu \rightarrow AN^*\cdots HO-Al \rightarrow ANH^{+}* + {}^{-}O-Al \quad (1)$$

It has been reported that the excited-state pK_a of acridine is 10.35,[28] much larger than for its ground state (pK_a = 5.45). This large change in pK_a has been explained as resulting from the acquisition of a higher electron density by the nitrogen heteroatom in the excited state than in the ground state, facilitating the proton addition reaction.[31] Thus, it is possible that on alumina surfaces, the excited state of hydrogen-bonded or neutral acridine reacts with the aluminol groups to produce the protonated form through a proton abstraction reaction (eq 1).

On the MgO surface, the acridine emission maximum (Figure 4d) appeared at 418 nm and the shape of the spectrum was similar to that observed for acridine dissolved in methanol (λ_{max} = 414 nm) and in water at pH of 10 (λ_{max} = 425 nm). Therefore, the hydrogen-bonded and neutral acridine species are postulated to be present on MgO.

The wavelengths of maximum emission of adsorbed protonated and neutral acridine differed by 50 nm (Figure 4a,d). As consequence, the emission spectra of adsorbed acridine can be utilized to estimate the average pH of the solid surface microenvironment. On the basis of this information, ammonium sulfate can be considered an acidic surface while magnesium oxide a basic surface. An excited-state photoprotolytic reaction occurred in acridine adsorbed on silica and alumina surfaces, which produced a high yield of protonated species. These photoprotolytic reactions would increase the emission fraction of ANH^+ (with respect to the values expected if no photoprotolytic reaction occurs), leading to a lower estimate of the pH value. Thus, to use acridine as a fluorescent probe to estimate the pH of these surfaces, the diffuse reflectance spectrum needs to be taken into consideration to prevent underestimating the pH. However, due to the contribution of ANH^+ to the steady-state absorption on silica and its absence from the spectra of acridine on alumina, we can expect that the hydroxyl groups on silica are more acidic.

The fluorescence of acridine is quenched by oxygen. In alkaline water, the decrease in fluorescence intensity under an oxygen atmosphere with respect to a nitrogen atmosphere was small, 0.93. However, on the solids surface the quenching of the fluorescence in the presence of oxygen was higher, 0.63 on silica, 0.54 on alumina, 0.51 on magnesium oxide, and 0.90 on ammonium sulfate, than in solution. The higher frequency of oxygen quenching on the solids than in solution is expected since acridine on the solid/air interface is more exposed to oxygen than in solution.

C. Time-Resolved Fluorescence Measurements. The fluorescence lifetimes of excited acridines in water at pHs of 2.5 and 9.0 and in methanol were obtained using the time domain fluorescence technique. These lifetimes increased with an increase of the emission wavelength. The shorter lifetimes were assigned to the neutral and hydrogen-bonded species, while the longer was assigned to the protonated species, which emit in the red side of the spectrum. The measured lifetimes (Table 1) were similar to those previously reported: 0.5 ns for acridine in methanol (AN···HO), 10−11 ns for acridine in alkaline water (AN), and 33.9 ns for acridine in acidic water (ANH^+).[18−20] Some of these decay lifetimes were measured in the presence of O_2 because insignificant oxygen quenching effects were observed.[18,20] In our studies, the solution and adsorbed samples of acridine were not flushed with N_2. Any difference between the observed lifetimes in solution included in Table 1 and those previously reported were probably due to differences in the data analysis. Lifetimes were also measured for acridine adsorbed on the different surfaces. By comparing these with those obtained in solution, the excited-state acridine species adsorbed were identified. Due to surface heterogeneity, two or more acridine species are postulated to be present on some surfaces, as demonstrated by the multiple component decay curves. Table 1 presents the lifetime (τ) of the fluorescent components on each surface at a given emission wavelength. In addition, the emission fraction (f) of each of the species contributing to the total emission is displayed. The emission fraction is the fraction of a species with a given lifetime that contributes to the total fluorescence.

The time-resolved emission spectra (TRES) of adsorbed acridine at different time delays were also recorded (Figure 6). This was done in order to assign the lifetimes to the spectra associated with different emitting species.

On silica gel, the TRES of acridine at short time delays was similar to the steady-state emission spectra, Figure 6a. A small band in the 410 nm region was observed at short time delays while at longer time delay (16 ns) was not observed. The fact that AN and AN···HO emit in this wavelength range, with lifetimes of 0.53 and 7.4 ns, respectively, explained the lack of emission from these species at longer time delays (Figure 6a). The longer time delay spectrum only showed an emission characteristic of ANH^+. The lifetimes obtained from the fits to the kinetic decay curves were similar to those observed for acridine in methanol (0.44 ns), alkaline water (8.5 ns), and acidic water (29 ns). The similarity between these lifetimes and those obtained for acridine adsorbed on silica led us to propose that AN···HO (0.53 ns), AN (7.4 ns), and ANH^+ (29.7 ns) are present on silica. In support of this, the fluorescence decay

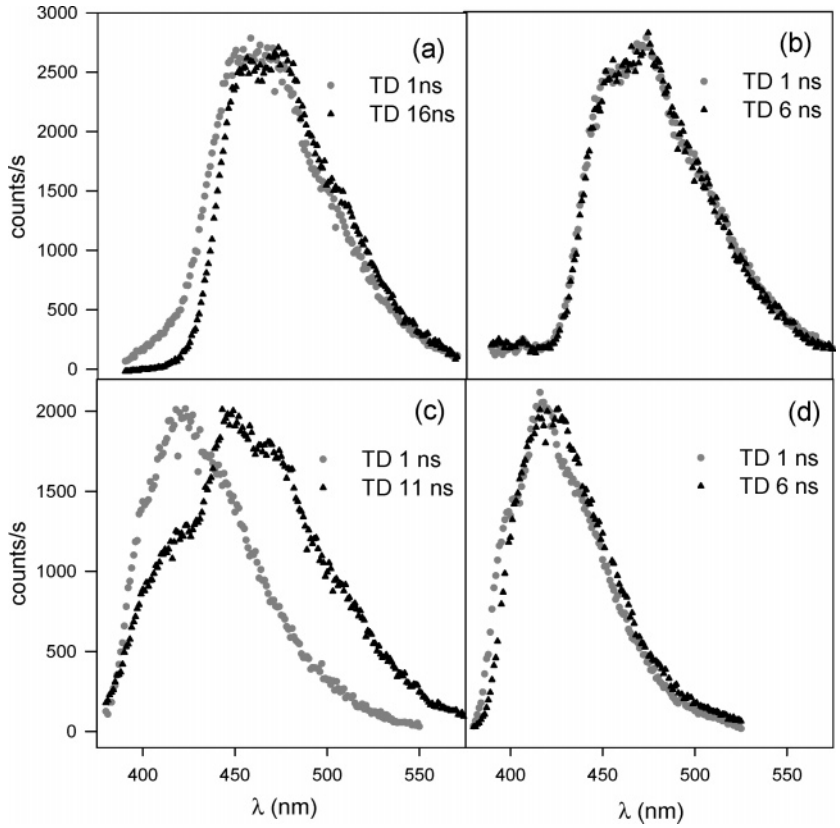

Figure 6. Time-resolved emission spectra of acridine on (a) 5×10^{-7} mol/g on SiO_2, (b) 5×10^{-8} mol/g on $(NH_4)_2SO_4$, (c) 6×10^{-7} mol/g on Al_2O_3, and (d) 5×10^{-6} mol/g on MgO at different time delays (TD).

TABLE 1: Time Domain Fluorescence Lifetimes (τ) and Emission Fractions (f) of Acridine Species in Solution and Adsorbed on Various Solids Surfaces

acridine medium and concn	emission wavelength (nm)	τ_1 (ns)	τ_2 (ns)	τ_3 (ns)	f_1	f_2	f_3
3×10^{-5} M methanol	412	0.44 ± 0.01			1.0		
3×10^{-5} M H_2O, pH = 9.1	425	8.5 ± 0.5			1.0		
3×10^{-5} M H_2O, pH = 2.5	470	29 ± 1			1.0		
5×10^{-7} mol/g SiO_2	425	0.53 ± 0.09	7.4 ± 0.4	25.6 ± 0.7	0.10 ± 0.05	0.35 ± 0.01	0.57 ± 0.01
	450	0.3 ± 0.2	6 ± 1	29.7 ± 0.3	0.01 ± 0.01	0.06 ± 0.03	0.93 ± 0.01
	470		5.4 ± 0.6	31.2 ± 0.2		0.05 ± 0.01	0.95 ± 0.01
	550			29.5 ± 0.1			1.0
5×10^{-8} mol/g $(NH_4)_2SO_4$	450	0.79 ± 0.05	2.6 ± 0.1		0.50 ± 0.4	0.51 ± 0.03	
	470	0.87 ± 0.03	2.9 ± 0.1		0.6 ± 0.4	0.38 ± 0.03	
	525	0.93 ± 0.04	3.0 ± 0.1		0.5 ± 0.3	0.51 ± 0.03	
6×10^{-7} mol/g Al_2O_3	410	0.83 ± 0.06	2.4 ± 0.3		0.74 ± 0.05	0.26 ± 0.07	
	425	0.96 ± 0.03	3.5 ± 0.3		0.80 ± 0.03	0.20 ± 0.02	
	444	0.87 ± 0.06	3.0 ± 0.2		0.55 ± 0.05	0.45 ± 0.04	
	480	1.48 ± 0.05	5.4 ± 0.2		0.58 ± 0.02	0.42 ± 0.02	
	530	1.84 ± 0.08	5.9 ± 0.2		0.47 ± 0.02	0.53 ± 0.02	
5×10^{-6} mol/g MgO	410	0.65 ± 0.03	3.1 ± 0.2		0.57 ± 0.07	0.43 ± 0.02	
	425	0.71 ± 0.03	3.6 ± 0.2		0.60 ± 0.04	0.40 ± 0.02	
	450	0.69 ± 0.03	3.0 ± 0.2		0.60 ± 0.04	0.40 ± 0.02	
	500	0.66 ± 0.03	3.4 ± 0.2		0.57 ± 0.05	0.43 ± 0.02	

curves for silica recorded at 425 and 450 nm were best fitted to a three-component system (Table 1). At 425 nm, the calculated lifetimes were characteristic of the AN···HO, AN, and ANH^+ species. At 450 nm the emission fractions associated with AN···HO and AN decreased in comparison to those obtained from the decay curve recorded at 425 nm. Since AN···HO (λ_{max} = 414 nm) does not emit at 470 and 550 nm, the data recorded at these emission wavelengths were best fitted to a two-component (AN and ANH^+) and one-component (ANH^+) system, respectively. The dependence of the emission fraction on the wavelength for each species correlated well with the emission spectra of the different acridine species. The species that emitted in the blue part of the spectra were those for which the emission fraction was inversely related to the magnitude of the detection wavelength.

For acridine adsorbed on ammonium sulfate, the TRES coincided with the ANH^+ emission spectrum observed in acidic water irrespective of the time delay used (Figure 6b). Contributions from the AN···HO or AN species were not observed in the emission spectra. This indicated that ANH^+ was the only adsorbed species present on ammonium sulfate. Nevertheless, the data were best fitted to a two-component model. This could have been due to the heterogeneity of the surface sites on which the ANH^+ is adsorbed. The fluorescence decay was faster (0.87

and 2.9 ns) than expected when compared to the fluorescence lifetime for ANH^+ in solution (29 ns) and on silica (29.5 ns). Also, the fluorescence intensity of acridine on ammonium sulfate was smaller than for acridine in acidic water. These effects are typical of quenching processes or a rapid photochemical reaction. However, since the emission wavelength range of the TRES was independent of the time delay an excited-state reaction did not explain the two-component decay. Therefore, quenching of the protonated acridines is a better explanation for the observations than the participation of an excited-state reaction. In addition, similar quenching effects had been observed by others for acridine in the presence of alcohols and ammonium nitrate.[18,32] Photophysical studies of acridine (AN) in alkaline water (pH 8.3) in the presence of ammonium ions have demonstrated the existence of proton addition reactions. However, the lifetime of the ANH^+ species formed from the photoprotolytic reaction with NH_4^+ was smaller (20 ns) than the characteristic lifetime of ANH^+ (30 ns) in the absence of the salt (NH_4NO_3).[32] This was explained in terms of quenching of the acridinium ion emission by NH_4NO_3.[32]

The TRES for acridine on alumina at (Figure 6c) short and long time delays were very different. At short time delays the TRES presented a $\lambda_{max} \sim 420$ nm, in the same wavelength region of the emission spectra of neutral and hydrogen-bonded acridine. Nevertheless, the TRES taken at longer time delays showed contributions from protonated acridine species. As already stated for the steady-state emission studies, this was due to the occurrence of a photoprotolytic reaction from the acridine singlet state. The analysis of the fluorescence decay curves for acridine on alumina at several emission wavelengths best fit a two-component model. In the wavelength emission region where the neutral and hydrogen-bonded acridine (410−440 nm) emit, the lifetimes of the two components were 0.83 and 3.0 ns. The shorter lifetime is characteristic of the hydrogen-bonded species, while the longer lifetime could be assigned to the neutral species. In the wavelength region where ANH^+ emits (480−530 nm) the measured lifetimes were 1.48 and 5.9 ns. Since these lifetimes were associated to ANH^+, which has a longer lifetime than AN···HO and AN, these were higher than those observed in the blue side of the emission spectra. However, the intrinsic lifetime of protonated acridine species were not observed. This is explained in terms of a similar pK_a of acridine and the aluminol groups. The proton abstraction from aluminol groups quenches the fluorescence of the acridines protonated in the excited state, resulting in a lower lifetime than the intrinsic lifetime of protonated acridine.

Excited acridine adsorbed on MgO showed two emission lifetimes at the emission maximum, 0.71 and 3.6 ns (Table 1). The presence of two species could be inferred from the TRES at the two time delays shown in Figure 6d. At shorter time delays the spectrum presented a wavelength of maximum emission near 417 nm, and its shape resembled that of hydrogen-bonded acridine. Moreover, at higher delays the recorded TRES was red-shifted with respect to that from short time delays. This is characteristic of a neutral acridine (AN in water at a pH of 9) whose spectrum is red-shifted (11 nm) with respect to the AN···HO emission spectrum. Therefore, neutral acridine was the species with a lifetime of 3.6 ns.

Studies of acridine in water−alcohol mixtures showed that the fluorescence lifetime decreased as the alcohol concentration increased due to a dynamic quenching process.[18] The possibility of interaction of neutral acridine with hydroxyl groups on the solids tested increased with an increment in their number on the surface; thus a decrease of the lifetime of neutral acridine resulted from the increase in the number of hydroxyl groups. Neutral acridine on silica showed a lifetime higher (7.4 ns) than on magnesium oxide (3.6 ns) or alumina (3.0 ns). This could be interpreted in terms of a smaller fraction of hydroxyl groups on the silica surface than on alumina and magnesium oxide. This agrees with the coverage of hydroxyl groups that is expected on these surfaces being higher in the alumina surface than in the silica surface.[20] The coverage of hydroxyl groups in thermally unactivated magnesium oxide had not been reported, but its known that it is covered with hydroxyl groups.[16]

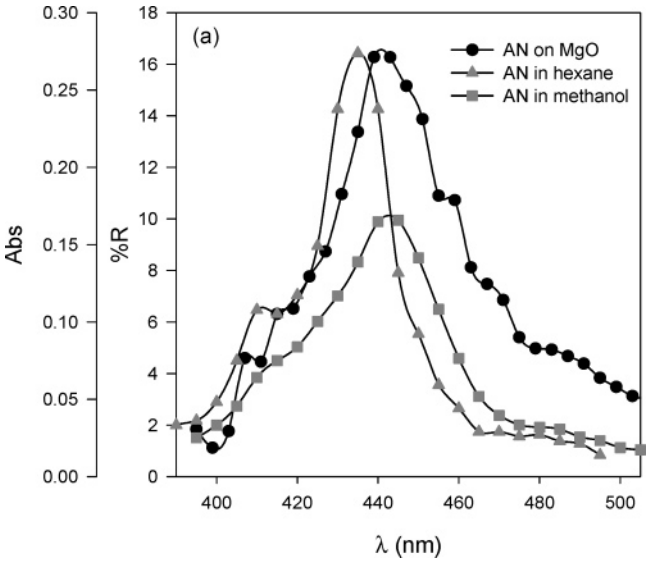

Figure 7. TRDR spectra of 1×10^{-5} mol/g acridine on MgO. For comparison the transient spectra of acridine in methanol and hexane are presented. An excitation wavelength of 355 nm was used.

D. Triplet−Triplet Absorption Spectra. The time-resolved diffuse reflectance (TRDR) spectroscopy technique was used to determine if the neutral, hydrogen-bonded, and protonated species undergo intersystem crossing to their triplet states when adsorbed on the surface of the solids tested and to assist in the characterization of the adsorbed species of acridine. These experiments were done in samples purged with nitrogen since the acridine triplet state is efficiently quenched by oxygen. Indeed, under an air atmosphere the T−T absorption of acridine was not seen. The wavelength of maximum absorption of triplet-state acridine in hexane and methanol has been reported as 435 and 441 nm, respectively.[21] The TRDR spectra of acridine adsorbed on MgO, Al_2O_3, and SiO_2 were obtained and compared with the transient spectra of acridine in solution.

For acridine adsorbed on MgO, the T−T absorption spectra showed a band with maximum at 441 nm (Figure 7). This is the same wavelength region where the triplet states of neutral acridine (in hexane, $\lambda_{max} = 435$ nm) and hydrogen-bonded acridine (in methanol, $\lambda_{max} = 443$ nm) absorb. Therefore, the neutral and hydrogen-bonded acridine triplet species were probably present. Moreover, the fact that the decay curves were best fitted to a two-component decay model with lifetimes 2×10^{-4} and 1×10^{-5} s supported the presence of these species. The triplet decay of the species adsorbed on the solids surface was slower than the decay observed in solution, 7×10^{-6} s in hexane and 1×10^{-5} s in methanol, due to less efficient internal conversion and quenching processes on the solids.

For acridine adsorbed on alumina (Figure 8a), the T−T absorption band appeared in the same wavelength region as for the triplet absorption of the neutral and hydrogen-bonded species, and the decay curves fit best to a one-component model with a lifetime of 1×10^{-4} s. This suggested that only one

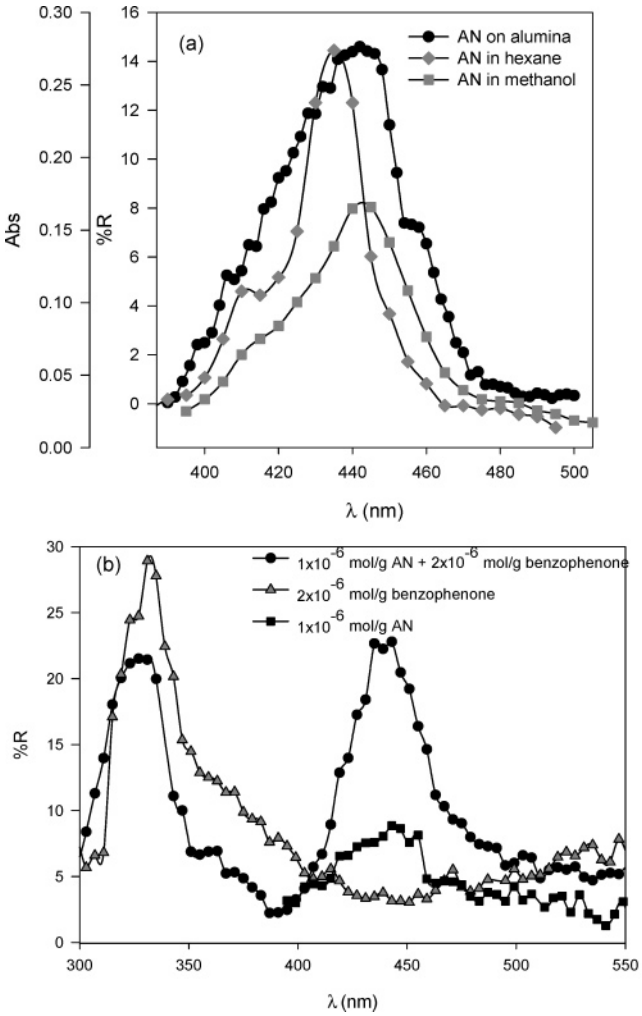

Figure 8. Transient absorption spectra of (a) 5×10^{-7} mol/g AN on alumina, 3×10^{-5} M AN in hexane, and 3×10^{-5} M AN in methanol. The excitation wavelength was 355 nm. (b) 1×10^{-6} mol/g AN and 2×10^{-6} mol/g benzophenone on alumina, 1×10^{-6} mol/g AN on alumina, and 2×10^{-6} mol/g benzophenone on alumina. The excitation wavelength was 266 nm.

type of species was present, although the presence of more than one species with closely spaced lifetimes could not be excluded. In the fluorescence studies the presence of protonated acridine was confirmed; nonetheless, absorption from the acridinium ion triplet state was not observed in the wavelength region where it absorbs (490 nm). Photoprotolytic reactions of the triplet state were not expected because its $^{T}pK_a$ is 5.6, very similar to the ground-state pK_a. Thus, deactivation of the singlet excited state of protonated acridine by intersystem crossing is not a major route.[22] Although the triplet state of these species can be sensitized by a disodium salt of naphthalene disulfonic acid, the triplet−triplet absorption by direct excitation of ANH^+ has not been observed in solution. This may be due to fluorescence and internal conversion processes which occur as the principal decay pathways.[22] If sensitized, the acridinium ion shows a T−T absorption band with maximum at 490 nm [22] that is approximately 45 nm red-shifted with respect to the T−T maximum absorption of neutral (hexane, $\lambda_{max} = 435$ nm) and hydrogen-bonded (methanol, $\lambda_{max} = 443$ nm) acridine species. Nonetheless, the identification of the triplet acridine protonated species produced by direct excitation has been reported on thermally activated alumina.[26] Internal conversion of the protonated species may be less efficient on the solid surface than in solution, resulting in a higher probability of intersystem crossing and observable T−T absorption.[26] Indeed, the fluorescence lifetime of ANH^+ on silica was higher than in acidic water, evidencing the less efficient internal conversion on the solids than in solution. To confirm the absence of ANH^+, benzophenone was used to sensitize the triplet state of the acridine species on alumina. The acridine triplet state was produced by sensitization from triplet benzophenone through an energy-transfer mechanism. As shown in Figure 8b, the T−T absorption of benzophenone at the 335 nm band diminished in intensity in the presence of coadsorbed acridine, while a transient absorption band of acridine at 445 nm increased demonstrating that acridine triplet sensitization was achieved. No significant increase in absorbance in the 490 nm region, in comparison with the T−T absorption spectra of nonsensitized triplet acridine, was observed. This indicated the absence of triplet-state protonated acridine on alumina.

At low surface loadings of acridine on silica, the triplet−triplet absorption decay curve presented a very low intensity, while at high surface loadings an intense delay fluorescence signal was observed. The latter overlapped with the acridine T−T absorption and resulted from T−T annihilation processes as previously reported by Oelkrug and collaborators.[26,33] They attributed it to the lateral motion of triplet acridines on the surface, rejecting the possibility of a nonuniform adsorption of the molecules on the surface. They also demonstrated that the acridine mobility on silica is higher than on alumina, resulting in T−T annihilation.[26] The higher mobility of acridine's triplet on hydroxylated silica was explained in terms of a smaller activation barrier for lateral motion than on hydroxylated alumina, on which the main adsorbate is protonated acridine trapped on the −OH groups. The alumina used in our studies was more basic than the silica, reducing delay fluorescence processes on that surface. The lack of absorption by ground-state protonated acridines on alumina further demonstrated the basicity of the surface. The high delay fluorescence detected from silica samples was ascribed to a low percent of hydroxyl groups per unit of surface area and a nonuniform adsorption of acridines that resulted from the method used to prepare the samples. The hydroxyl groups could form hydrogen bonds with the acridines resulting in a higher strength of interaction between the acridines and the surface. This would decrease the mobility of the acridines. In addition, a nonuniform adsorption is more likely on silica than on alumina due to the lower amount of hydroxyl groups on the latter,[15] which are the main sites for the adsorption of azaaromatics.[25,26] The delay fluorescence spectrum of acridine on silica was in the region where protonated species emit (Figure 9). Therefore, these species are the precursors to T−T annihilation processes. Because the triplet state of the species must be populated before delay fluorescence occurs, protonated acridines may undergo intersystem crossing to their triplet state on silica. The formation of triplet-state protonated acridines may be the result of the less efficient internal conversion on the solid surface than in solution, resulting in a higher probability of intersystem crossing and observable T−T absorption.[26] In experiments using silica in which the acridine triplet was produced by benzophenone, the delay fluorescence was less intense, which allowed the triplet−triplet absorption intensity to be recorded at times where the delay fluorescence had decayed completely (Figure 10). Additionally on this substrate, a decrease in the absorption intensity of benzophenone with a simultaneous growth of the acridine's triplet absorption was observed. Analysis of the decay curve of the acridine triplet absorption on silica showed the presence of one species. However, an analysis of the fluorescence decay

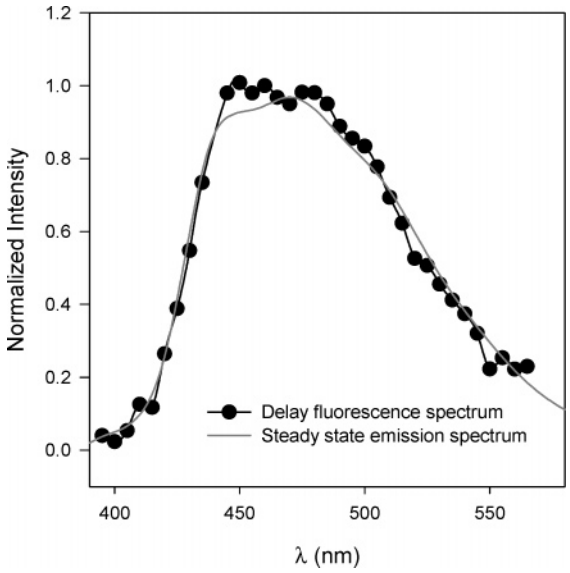

Figure 9. Transient delay fluorescence spectra of 1×10^{-6} mol/g acridine on silica. The excitation wavelength was 355 nm.

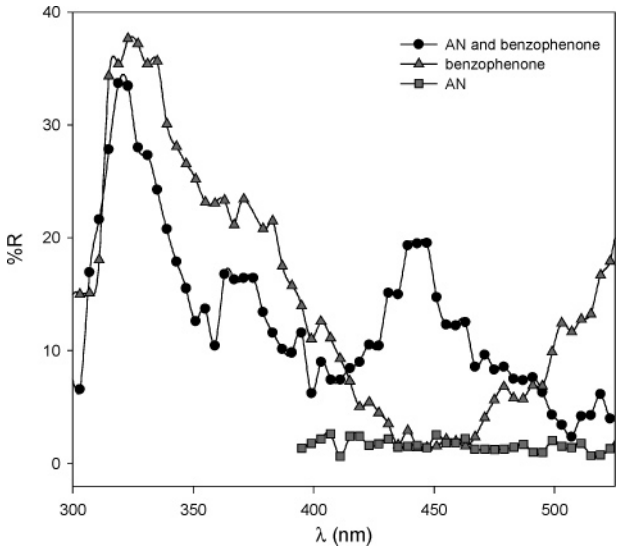

Figure 10. TRDR spectra of 1×10^{-6} mol/g AN and 2×10^{-6} mol/g benzophenone on silica, 1×10^{-6} mol/g AN on silica, and 2×10^{-6} mol/g benzophenone on silica. The excitation wavelength was 266 nm.

curves demonstrated that three species were present on silica, ANH^+, AN···HO, and AN. It is possible that the triplet states of more than one species with similar lifetimes were present on silica. The shoulder at the 485 nm region (Figure 10) implied the possible absorption by triplet-state protonated acridine. For acridine and benzophenone coadsorbed on silica, the triplet decay curves at the 485 nm region showed a slower decay than those from the sample of benzophenone on silica. This further demonstrates that the transient absorption observed at the 485 nm region is due to the absorption from protonated acridines.

No transient signals for acridine adsorbed on ammonium sulfate were observed. Moreover, no T−T absorption of acridine using benzophenone as a triplet sensitizer was observed and the T−T absorption of benzophenone was extremely low in intensity. This supported the hypothesis that a rapid quenching of excited acridine with the surface was occurring.

E. Photodegradation Rates. In water, the photodegradation rate was 3.2 times higher for the neutral than for the protonated acridine species because neutral acridines (AN···HO and AN) can undergo intersystem crossing while for the ionic acridines (ANH^+) that is not an important deactivation route. For neutral species the photodegradation rate was 0.12 lower under an oxygen than under a nitrogen atmosphere, suggesting the role of the singlet and triplet excited states in the destruction of acridine. Under a nitrogen atmosphere, the ratio of the photodegradation rates on ammonium sulfate, magnesium oxide, and alumina to that on silica (the slowest observed) was 107 on ammonium sulfate, 25 on magnesium oxide, and 18 on alumina. The slower photodegradation rates, observed for acridine on SiO_2, Al_2O_3, and MgO surfaces, can be explained in terms of the presence of ANH^+. As its relative proportion increased on the different surfaces, the photodegradation rate also decreased. It was higher on magnesium oxide, a surface at which no ANH^+ is present. On alumina, no ground-state ANH^+ species were observed; however, excited-state proton addition reactions occurred. These reactions decrease the quantity of AN that can undergo intersystem crossing processes to their triplet states resulting in a lower photodegradation rate. On silica, ground-state protonated acridines were present and a photoprotolytic reaction occurred; therefore, the acridine photodegradation rate on silica was slower than on magnesium oxide and alumina. However, the protonated species on silica were shown to undergo intersystem crossing to their triplet state, but due to their high mobility on silica these can undergo T−T annihilation, which deactivates the triplet excited state. Ammonium sulfate was the surface on which acridine degraded faster. This was an unusual behavior because on this surface the protonated acridine was the principal adsorbed species present. This unusual behavior was also observed in the photophysical studies of acridine on ammonium sulfate. At a similar initial absorbance, the fluorescence intensity of acridine on ammonium sulfate was smaller than for acridine in acidic water or adsorbed on a silica surface. In addition, the fluorescence lifetimes of acridine on ammonium sulfate were 15 times lower than for acridine in acidic water, implying that a dynamic fluorescence quenching process could occur. Therefore, the unusual high photodegradation rate is explained in terms of an excited-state reaction of acridine with the surface. On all surfaces the photodegradation under a N_2 atmosphere was faster than under an O_2 atmosphere except for acridine on ammonium sulfate where the photodegradation rates under a N_2 and O_2 atmosphere were similar. This correlates well with the absence of a triplet decay route for the adsorbed species as evidenced by the absence of acridine T−T absorption on ammonium sulfate.

IV. Summary

Several photophysical and photochemical processes are proposed to occur for neutral, hydrogen-bonded, or protonated acridine species adsorbed on the models of atmospheric particulate matter used in this study. The processes that occur will depend on the adsorbed acridine species on each model surface. For acridine on silica, the ground-state species present were the hydrogen-bonded, neutral, and protonated. These species were characterized from the steady-state diffuse reflectance spectrum, and the analysis of the emission decay curves of acridine confirmed the presence of AN and AN···HO. Because the pK_a of the acridine singlet excited state is greater than for its ground and triplet states, a photoprotolytic reaction could explain the much higher emission fraction of ANH^+ with respect to AN and AN···HO on silica. On ammonium sulfate, the diffuse reflectance, emission, and time-resolved emission spectra showed that protonated acridine was the only adsorbed species. Because the fluorescence lifetimes and fluorescence intensity were smaller than expected (from the spectroscopic

characteristics of ANH^+ in acidic water), we propose that quenching of the excited-state acridine was occurring. On alumina, the presence of hydrogen-bonded species was supported by steady-state and time-resolved diffuse reflectance measurements. Possibly the neutral acridine species was also present on alumina. The fluorescence and TRES showed that the ANH^+ species have been formed through a photoprotolytic reaction. For acridine on magnesium oxide, the presence of the neutral and hydrogen-bonded species were clearly established from the two-component analysis of the fluorescence and T−T absorption decay curves and the TRES at different time delays. This was the only solid surface where neither the ground-state nor excited-state acridine-protonated species were observed probably because of the higher pH of the magnesium oxide surface. A dependence of the acridine photodegradation rate on the different solids with respect to the type of adsorbed species and nature of the surface was observed. In general, neutral species have a higher photodegradation rate than the protonated species, photoprotolytic reactions and T−T annihilation are proposed to decrease the photodegradation rate, and the unusual high photodegradation rate observed on ammonium sulfate may be due to a reaction with the surface.

V. Conclusions

The diverse composition of the atmospheric particulate matter probably permits the presence of all acridine species on the surface of particles. These studies on model surfaces suggest that the acidity and nature of the atmospheric particulate will determine the presence of particular adsorbed acridine ground-state species and the excited states (triplet and/or singlet) which are subject to photodegradation. Photodegradation through the triplet and singlet states can occur for neutral and hydrogen-bonded acridine, while for protonated acridine the main reactive state is the singlet state. Photoprotolytic reactions could occur on atmospheric particulates if the acidity of the hydroxyl groups on the surface is between the pK_a of the ground state and singlet excited state. These types of reactions will decrease the quantity of hydrogen-bonded and/or neutral acridines that can undergo intersystem crossing to their triplet states, resulting in a decrease of the frequency of degradation via the triplet state.

Acknowledgment. Dr. Rolando Oyola is acknowledged for laser flash spectrophotometer programming, and the financial support, by the National Science Foundation (Grant HRD981-7642), United States Department of Energy, and the NIH-SCORE (Grant 5S06GM08102) programs.

Supporting Information Available: The diffuse reflectance spectra of acridine on alumina under an oxygen and nitrogen atmosphere, to demonstrate that the oxygen does not have a strong effect in the absorption by acridine. This material is available free of charge via the Internet at http://pubs.acs.org.

References and Notes

(1) Leiter, J.; Shimkin, M. B.; Shear, M. J. *J. Natl. Cancer Inst.* **1942**, *3*, 155.
(2) Daisey, J. M. Organic Compounds in Urban Aerosols. In *Aerosols: Anthropogenic and Natural, Sources and Transport*; Kneip, T. J., Lioy, P. J., Eds.; The New York Academy of Sciences: New York, 1980; Vol. 338, p 50.
(3) Warshawaski, D.; Barkeley, W.; Bingham, E. *Fundam. Appl. Toxicol.* **1993**, *20*, 376.
(4) Bocedas, L.; Roment, L.; Toff, E.; Jenssen, D.; de Pierre, J. W.; Ahbert, M. B. *Reprod. Toxicol.* **1993**, *7*, 219.
(5) Wiegman, S.; Van Vlaardingen, L. A.; Peijnenburg, G. M.; Van Beusekom, A. M.; Kraak, H. S.; Admiraal, W. *Environ. Sci. Technol.* **1999**, *33*, 4256.
(6) Handa, T.; Yamauchi, T. *Environ. Sci. Technol.* **1987**, *12*, 1177.
(7) Ostman, L.; Carlsson, H. J. *J. Chromatogr. A* **1997**, *790*, 73.
(8) Meylan, W. M.; Howard, P. H. *Environ. Sci. Technol.* **1991**, *10*, 1283.
(9) Banwart, W. L. *Soil Sci.* **1982**, *133*, 42.
(10) Swann, R. L. *Res. Rev.* **1983**, *85*, 23.
(11) Kasama, K.; Kikuchi, K.; Nishida, Y.; Kokubun, H. *J. Phys. Chem.* **1981**, *85*, 4148.
(12) Kellmann, A. *J. Chem. Phys.* **1977**, *81*, 1195.
(13) Tokumura, K.; Kikuchi, K.; Koizumi, M. *Bull. Chem. Soc. Jpn.* **1973**, *46*, 1309.
(14) Finlayson-Pitts, B. J.; Pitts, J. N. *Chemistry of the Upper and Lower Atmosphere: Theory, Experiments and Applications*; Academic Press: San Diego, CA, 2000.
(15) Jonhston, L. J. Phototransformations of organic molecules adsorbed on silica and alumina. In *Photochemistry in Organized and Constrained Media*; Ramamurthy, Ed.; VCH Publishers: New York, 1991; p 359.
(16) Foster, M.; Furse, M.; Passno, D. *Surf. Sci.* **2002**, *502*−*503*, 102.
(17) Weis, D. D.; Ewing, G. E. *J. Geophys. Res.* **1996**, *101*, 18709.
(18) Ito, O.; Ito, E.; Yoshikawa, Y.; Watanabe, A.; Kokubun, H. *J. Chem. Soc., Faraday Trans.* **1996**, *92*, 227.
(19) Kasama, K.; Kikuchi, K.; Yamamoto, S.; Uji-ie, K.; Nishida, Y.; Kokubun, H. *J. Phys. Chem.* **1981**, *85*, 1291.
(20) Kokubun, H. *Bull. Chem. Soc. Jpn.* **1969**, *42*, 919.
(21) Barrio, J. I.; Rebato, J. R.; Tablas, F. M. G. *Chem. Phys. Lett.* **1988**, *149*, 150.
(22) Nishida, Y.; Kikuchi, K.; Kokubun, H. *J. Photochem.* **1980**, *13*, 75.
(23) Smirnova, N. P.; Samchuk, S. A.; Yeremenko, A. M.; Chuiko, A. A. *J. Mol. Struct.* **1990**, *218*, 453.
(24) Uhl, S.; Oelkrug, D. *J. Mol. Struct.* **1988**, *175*, 117.
(25) Smirnova, N. P.; Yeremenko, A. M.; Bykovskaya, L. A.; Kulikov, S. G.; Chuiko, A. A. *J. Mol. Struct.* **1992**, *266*, 417.
(26) Oelkrug, D.; Uhl, S.; Wilkinson, F.; Willsher, C. J. *J. Phys. Chem.* **1989**, *93*, 4551.
(27) Rempfer, K.; Uhl, S.; Oelkrug, D. *J. Mol. Struct.* **1984**, *114*, 225.
(28) Uhl, S.; Rempfer, K.; Egelhaaf, H. J.; Lehr, B.; Oelkrug, D. *Anal. Chem. Acta* **1995**, *303*, 17.
(29) Lloyd, J. B. F. *Analyst* **1975**, *100*, 529.
(30) Birks, J. B. *Photophysics of Aromatic Molecules*; Wiley-Interscience: London, 1970.
(31) Bowen, E. J.; Holder, H. J.; Woodger, G. B. *J. Phys. Chem.* **1962**, *66*, 2491.
(32) Lakowicz, J. R.; Balter, A. *Biophys. Chem.* **1982**, *16*, 117.
(33) Oelkrug, D.; Gregor, M.; Reich, S. *Photochem. Photobiol.* **1991**, *54*, 539.